Supplementary Information

Contents

1. MAIN FINDINGS OF THIS WORK

Noise in biological systems could be expected to influence many processes in the cell, particularly the ones where a defined output has to be produced upon certain stimulus, as in signal transduction (see main text). Using chemotaxis in *Escherichia coli* as a model system, we combined experimental analysis with mathematical modelling to analyse the robustness of the signal transduction pathway to a stochastic intercellular variation in protein levels. The design of the chemotaxis pathway (Fig. 1c) and the regulation of expression of chemotaxis genes (Fig. S1a) are well understood. We used fusions to yellow and cyan fluorescent proteins (YFP and CFP) as translational reporters to measure variation in the levels of chemotaxis proteins in a cell population (Fig. 2). We observed a strong co-variation in the single-cell levels and only a weak uncorrelated variation (Fig. S1b, Fig. 2b). Moreover, the variation decreased at a higher rate of transcription. Both findings are consistent with an assumption that such variation, or gene expression noise, is mainly determined by transcription [1]. Using mathematical analysis, we found that the experimentally established design of the chemotaxis pathway (Fig. 1c) is robust to concerted variation in protein levels and predicted that the variation in the output of the pathway, the level of phosphorylated CheY (CheY-P), should be much smaller than the variation in the levels of chemotaxis proteins (Fig. S1c). Such robustness would enable most individuals in the population to be fully chemotactic - that is to have the level of CheY-P in the working range of flagellar motor. This prediction was confirmed experimentally by showing that the cells remain chemotactic and keep CheY-P concentration in the right range upon an up to 6.6-fold overexpression of all chemotaxis proteins. We speculate that the robustness to gene expression noise provides an advantage to a population and is thus under evolutionary selection.

2. DESCRIPTION OF THE MATHEMATICAL MODELLING

2.1. Brief Introduction to Bacterial Chemotaxis

Signal transduction networks have to transmit information in a robust way but tolerate only small variations of the output to a given input signal. One of the best-studied simple signalling systems is bacterial chemotaxis, which allows bacteria to navigate in gradients of chemical attractants or repellents. Here, information about ambient changes in chemo-ligand are transmitted from receptors on the cell surface to the flagellar motors by a stimulation-dependent phosphorylation of a diffusible response regulator protein CheY. Most biochemical rate constants and average concentrations of chemotaxis proteins under standard conditions have been determined [2, 3], making chemotaxis an excellent system for a quantitative analysis. Another advantage of the chemotaxis pathway is its relative isolation from other cellular processes, such as metabolism, which allows treating the pathway as an independent module [4]. Chemotaxis pathways can sense relative changes of attractant concentrations as small as two percent over a dynamic concentration range of five orders of magnitude [5]. Previous quantitative analysis showed that such a large dynamic range can be explained by a combination of allosteric signal amplification by receptor clustering [6] and

a precise adaptation mechanism (c.f Refs. [7–10]). Precise adaptation is the ability to return to the same level of pathway activity under conditions of continuous stimulation. Failure of this systems property would lead to permanently swimming or tumbling behaviour and thus to the loss of the chemotactic ability. In *E. coli*, sudden addition of attractant leads to an instantaneous decline in receptor activity followed by a slow adaption process. There is strong evidence that precise adaptation is a direct consequence of a reversible methylation process of the receptors sensing chemo-ligands. In this process a higher level of methylation increases the probability of a receptor to switch to an active state [5]. Almost perfect adaption results from a constantly working methyltransferase (CheR) balanced by a methylesterase (CheB), which works only on active receptors [11]. Active receptors enhance autophosphorylation activity of CheA, which in turn phosphorylates CheY.

2.2.   Two-State Model of Bacterial Chemotaxis

The mathematical description used in this work to simulate the dynamics of a chemotactic signalling system relies on following assumptions:

1. The numbers of protein copies are sufficiently large, such that stochastic effects on the protein level can be neglected

2. Each stable receptor complex includes one kinase protein, CheA.

3. A receptor complex can exist only in two functional states, active or inactive (two-state model) [7]

4. The rate of CheA phosphorylation is assumed to be proportional to the average number of active receptor complexes in the cell

5. The protein-protein interactions can be described by Michaelis-Menten kinetics

The probability, $p_m(L)$, of receptor in methylation state $m \in \{0, 1, 2, 3, 4\}$ to be active in an ambient attractant concentration L is given by

$$p_m(L) = V_m \left(1 - \frac{L^{H_m}}{L^{H_m} + K_m^{H_m}} \right) \tag{S1}$$

The response amplitudes, V_m, Hill coefficients, H_m, and the values at half maximum response, K_m, used throughout this work are taken from Ref. [5] and are listed in Table S2.

We emphasise that none of the results derived in this work depends on the precise values of these coefficients.

The time-evolution of the different phosphorylation and methylation states for the topologies Fig. 1 follows along the lines of Rao et al (c.f. Ref. [12]) and are described by the following equations:

Sites methylated	$K_m[mM]$	H_m	V_m
0	$27 \cdot 10^{-4}$	1.2	0.0
1	$20 \cdot 10^{-3}$	1.2	0.25
2	$150 \cdot 10^{-3}$	1.2	0.5
3	$150 \cdot 10^{-2}$	1.2	0.75
4	60	1.2	1

TABLE S1: Parameters for response of receptors in different methylation states to attractant (α-methyl-DL-aspartate).

Topology Fig. 1a:

$$\partial_t T_m = k_R R \frac{T_{m-1}}{K_R + T^T} + k_B B \frac{T^A_{m+1}}{K_B + T_A} \tag{S2}$$

$$- k_R R \frac{T_m}{K_R + T^T} - k_B B \frac{T^A_m}{K_B + T_A}$$

$$\partial_t Ap = k_A \left(A^T - Ap \right) T_A - k_Y Ap \left(Y^T - Yp \right) \tag{S3}$$

$$\partial_t Yp = k_Y Ap \left(Y^T - Yp \right) - \gamma_Y Yp \tag{S4}$$

Topology Fig. 1b:

$$\partial_t T_m = k_R R \frac{T_{m-1}}{K_R + T^T} + k_B B \frac{T^A_{m+1}}{K_B + T_A} \tag{S5}$$

$$- k_R R \frac{T_m}{K_R + T^T} - k_B B \frac{T^A_m}{K_B + T_A}$$

$$\partial_t Ap = k_A \left(A^T - Ap \right) T_A - k_Y Ap \left(Y^T - Yp \right) \tag{S6}$$

$$\partial_t Yp = k_Y Ap \left(Y^T - Yp \right) - k_Z Yp Z - \gamma_Y Yp \tag{S7}$$

Topology Fig. 1c:

$$\partial_t T_m = k_R R \frac{T_{m-1}}{K_R + T^T} + k_B Bp \frac{T^A_{m+1}}{K_B + T_A} \tag{S8}$$

$$- k_R R \frac{T_m}{K_R + T^T} - k_B Bp \frac{T^A_m}{K_B + T_A}$$

$$\partial_t Ap = k_A \left(A^T - Ap \right) T_A - k_Y Ap \left(Y^T - Yp \right) \tag{S9}$$

$$- k'_B Ap \left(B^T - Bp \right)$$

$$\partial_t Yp = k_Y Ap \left(Y^T - Yp \right) - k_Z Yp Z - \gamma_Y Yp \tag{S10}$$

$$\partial_t Bp = k'_B Ap \left(B^T - Bp \right) - \gamma_B Bp \tag{S11}$$

Topology Fig. 1d:

$$\partial_t T_m = k_R R \frac{T_{m-1}}{K_R + T^T} + k_B Bp \frac{T^A_{m+1}}{K_B + T_A} \tag{S12}$$

$$- k_R R \frac{T_m}{K_R + T^T} - k_B Bp \frac{T^A_m}{K_B + T_A}$$

$$\partial_t Ap = k_A \left(A^T - Ap \right) T_A - k_Y Ap \left(Y^T - Yp \right) \tag{S13}$$

$$- k'_B Ap \left(B^T - Bp \right)$$

$$\partial_t Yp = k_Y Ap \left(Y^T - Yp \right) - k_Z Yp\, Z^* - \gamma_Y Yp \tag{S14}$$

$$\partial_t Bp = k'_B Ap \left(B^T - Bp \right) - \gamma_B Bp \tag{S15}$$

$$\partial_t Z^* = k^*_Z Yp \left(Z^T - Z^* \right) - \gamma^*_Z Z^* \tag{S16}$$

The concentration of receptor complexes with m residues methylated are denoted by T_m and $T_A = \sum_m T^A_m$ is the concentration of active receptors, with $T^A_m = p_m(L)\, T_m$. In topology Fig. 1d, the rate of activation of CheZ by CheY-P is denoted by k^*_Z and the corresponding decay rate by γ^*_Z. There is indirect experimental evidence [13] for an active form of the CheY phosphatase (Z^*). All other protein concentrations are denoted as in the main text. One should note that the above defined equations show only precise adaption if the highest methylation state is not significantly populated. Latter restriction can be lifted if one allows the methyltransferase to work exclusively on inactive receptors [11]. It has been shown for *E. coli in vitro* [14] and *in vivo* [5] that changing an attractant occupancy of just a few receptors out of thousands elicits a much larger change in kinase activity. There is increasing evidence that this signal amplification (gain) in bacterial chemotaxis can be explained by long-range allosteric interactions between receptors localised at the cell poles [15–20]. To account for the receptor interactions in a simple way, we assume that kinase activity depends linear on the concentration of all active receptors. Thus, the first term in Eq. (S9) does not reflect a bimolecular reaction but accounts for the strong non-linear relation between receptor occupancy with ligand and kinase activity in a mean field approximation [20] and also accounts for the experimental finding that a two-fold increase in aspartate or serine receptors at fixed methylation levels results in a four-fold increase in kinase activity [17].

The average concentrations of the chemotaxis proteins are taken from Ref. [2] for the strain RP437 assuming a cell volume of 1.4 fl: [CheA]= 5.3 μM, [CheY]= 9.7 μM, [CheB]= 0.28 μM, [CheR]= 0.16 μM, [CheZ]= 3.8 μM. The concentration of the receptor complexes is set equal to [CheA].

2.3. Determination of Kinetic Constants used in Simulations

The kinetic rates and Michaelis-Menten constants of the methylation process are determined such that the maximum number of bacteria in a population show accurate chemotactic response under physiological intercellular variations in protein concentrations (Fig. 2). The protein concentrations for the individuals in a population are generated by the random

process, Eq. (S17),

$$x_i = \langle x_i \rangle_{wt} \left(\lambda r_{ex} + \nu \sqrt{\lambda r_{ex}} \, \xi_i^{(2)} \right) \qquad \text{(S17)}$$

$$\approx \langle x_i \rangle_{wt} \left(\lambda r_{ex} + \nu \sqrt{\lambda} \, \xi_i^{(2)} \right) \quad , \qquad \text{(S18)}$$

with x_i the protein concentrations of the i-th chemotaxis protein and $\langle x_i \rangle_{wt}$ the corresponding average concentration of x_i for the strain RP437, as given before. The factor of overexpression is denoted by λ. The co-variations follow a log-normal distribution given by $r_{ex} = N_r \exp[\alpha \, \xi^{(1)} \ln 10]$ with N_r chosen such that $\langle r_{ex} \rangle = 1$, and $\xi^{(1)}$ and $\xi^{(2)}$ are normally distributed random variables with mean zero and variance one. The values $\nu = 0.20$, $\alpha = 0.20$ reproduce gene expression noise measured in Fig. 2a and Fig. 2b, respectively (see also Fig. S2). The decrease of uncorrelated variations with $\eta_{in} \sim \lambda^{-1/2}$ assumes that protein syntheses follows a Poisson process and proteins are expressed from polycistronic mRNA (see Ref. [1]). This is confirmed by co-expression of CheY-YFP and CheZ-CFP as a single transcript from a plasmid (pVS88) at different levels of IPTG induction (Table S2 and Fig. S3). The population size used in the simulations are 70 individuals for the determination of the kinetic constants and 10^4 individuals for quantifying the fraction of fully chemotactic bacteria (Fig. 3 and Fig. 4).

λ	η_{ex}	η_{in}	$\eta_{in}^{theo} = \eta_{in}^{wt} n^{-1/2}$
1	0.44	0.20	0.20
2.52	0.27	0.15	0.13
14.1	0.21	0.067	0.053

TABLE S2: Gene expression noise of CheY-YFP and CheZ-CFP expression from a single IPTG-inducible promoter at 0μM, 5μM, and 10μM IPTG. Mean expressions relative to the wild type are denoted by λ. The correlated and uncorrelated contributions of gene expression noise, η_{ex} and η_{in}, decline for higher expression levels and latter agrees with the theoretical predicted values from the model Eq. (S18), $\eta_{in}^{theo} = \nu \lambda^{-1/2}$, with $\nu = \eta_{in}^{wt} = 0.20$ the uncorrelated part of gene expression noise for the wild type.

The following rate constants are estimated from various measurements found in the literature [3]. The CheA autophosphorylation rate mediated by active receptors is set to $k_A = 50\mu\text{M}^{-1}s^{-1}$. The CheY phosphorylation by phosphotransfer from CheA to CheY has the value $k_Y = 100\mu\text{M}^{-1}s^{-1}$. The dephosphorylation rate for CheY are given by $k_Z = 30/[\text{CheZ}]\text{s}^{-1}$ and $\gamma_Y = 0.1$ for the topologies Fig. 1b, 1c, 1d and $\gamma_Y = 30.1$ for topology Fig. 1a. For the topologies Fig. 1c, 1d the optimal value for [CheB-P] can be determined from an optimisation procedure for highest chemotactic performance as described below, but the outcome is essentially that CheB-P takes the smallest possible value (see section 2.6.4). We therefore adjust the rate of CheB phosphorylation such that [CheB-P] is about one fourth of the total concentration of CheB. This essentially results in a four-fold higher demethylation activity. Furthermore, for CheB activation we

set $k_B' = 3\mu\text{M}^{-1}s^{-1}$ with corresponding auto-dephosphorylation rate $\gamma_B = 1s^{-1}$. For the active form $CheZ^*$ in topology Fig. 1d a four-fold higher phosphatase activity is assumed in comparison to CheZ in topologies Fig. 1a-c.

The rate constants for the methylation process and the CheY-CheZ feedback of topology Fig. 1d are determined by an optimisation procedure [21] towards highest chemotactic performance with parameters given above to result in an adaptation time of 100s after sudden addition of attractant (35μM α-methyl-DL-aspartate) and an adaptation time of 25s after removal. A further condition is a fixed adapted concentration of phosphorylated CheY which is set to 3.2μM (2.8μM for Fig. 3b) [22]. We determined the optimal rate and Michaelis-Menten constants by minimising the quadratic functional

$$E[\mathbf{k}, \mathbf{K}] = \min \frac{1}{N} \sum_{i=1}^{N} \left[\sum_{l=1}^{N_L} \frac{\left(Yp_l^{(i)} - Yp^*\right)^2}{N_L \sigma_Y^2} + \frac{\left(\tau_1^{(i)} - \tau_1^*\right)^2}{2\sigma_1^2} + \frac{\left(\tau_2^{(i)} - \tau_2^*\right)^2}{2\sigma_2^2} \right] \tag{S19}$$

with $\tau_1^* = 100s$, $\tau_2^* = 25s$, and $Yp^* = 1/3\,Y^T$. Because precise adaption is the outstanding feature of the chemotaxis pathway it is reasonable to assume that a higher selective pressure is given for the precise regulation of CheY-P than for adaptation times. In the simulations we use the standard deviations, $\sigma_Y = 1/6\,Yp^*$, $\sigma_1 = 1/2\,\tau_1^*$ and $\sigma_2 = 1/2\,\tau_1^*$ but for the general conditions that σ_Y/Yp is significantly smaller than σ_1/τ_1^* and σ_2/τ_2^* we arrive essentially at the same results as for the specific standard deviations above (data not shown). The sum runs over N individuals whose protein concentration are generated from the random process, Eq. (S17), and $N_L = 3$ denotes the number of stepwise increments of attractant to show maximum response.

The result of the optimisation procedure for the different topologies in Fig. 1 is given in Table S3. For the topology Fig. 1d the kinetic constants for the CheY-CheZ feedback loop has been optimised by the same procedure and are given in table S4.

Topology	k_R [$\mu M^{-1}s^{-1}$]	K_R [μM]	k_B [$\mu M^{-1}s^{-1}$]	K_B [μM]
Fig. 1a	0.5	0.062	16	16
Fig. 1b	1.0	0.043	16	10.1
Fig. 1c	0.39	0.099	6.3	2.5
Fig. 1d	0.39	0.099	6.3	2.5

TABLE S3: Kinetic constants of the methylation process for the different topologies Fig. 1.

Topology	k_Z^* [$\mu M^{-1}s^{-1}$]	k_Z [$\mu M^{-1}s^{-1}$]	γ_Z [s^{-1}]
Fig. 1d	1.33	$3.64 \cdot 10^2$	$2.20 \cdot 10^2$

TABLE S4: Kinetic constants of the CheY-CheZ feedback loop in Fig. 1d.

We emphasise that the outcome of CheR working at saturation is direct consequence of the model assumption that prefect adaptation is due to an integral feedback loop at the methylation level. The higher chemotactic efficiency resulting from compensation for co-varying protein levels then drives the Michaelis-Menten constant for the methyltransferase to small values. But one should note that the experimentally found value of $K_R^{ex} = 10 \mu M$ [3] is in accord with the optimisation result of saturation behaviour for CheR as the receptor concentration within the poles can be estimated to be $\sim 200 \mu M$ and is therefore significantly larger than K_R^{ex}.

2.4. Robustness against Variations in Transcriptional Activity

In this section we derive the necessary conditions for a chemotaxis pathway to be robust against variations in transcriptional activity. Transcriptional noise leads to co-variation of expression-levels within the same operon, as shown in Fig. 2b, Figs. S2 and S3, and Table S2. The extend of these co-variations can be up to ten-fold of the wild type gene expression [2]. Bacterial populations showing chemotactic response among all their individuals are selective advantageous to bacteria which lose their chemotactic ability under such variations in gene expression. Thus, the topology of the chemotaxis pathway should have evolved in such a way that the steady state concentration of the response regulator protein CheY-P is invariant under a λ-fold increase in transcriptional activity.

The time evolution of a spatial homogeneous biochemical network can be described by a set of ordinary differential equations. Let $\{y_1(t), \ldots, y_N(t)\}$ be the concentrations of the N different states of the proteins involved in the pathway. Summation over all different states of the protein with index k results in the total concentration $x_k^T = \sum_{\{y_i\}_k} y_i$. Since the dynamics of the chemotaxis pathway ranges on time scales from 10^{-2} seconds to minutes, and the turnover time for proteins is significantly larger in bacteria, we can assume the total concentration of the chemotactic proteins to be constant, $x_k^T \approx const$, for the time scales a cell needs to climb a gradient in ligand concentration.
Thus, the differential equations describing the dynamics of the chemotaxis pathways shown in Fig. 1 have the functional form

$$\partial_t y_i(t) = F_i(\mathbf{y}(t)|\mathbf{x}^T) \tag{S20}$$

The steady state solution $F_i(\mathbf{y}(t)|\mathbf{x}^T) = 0$ is invariant under a λ-fold increase of transcriptional activity $\mathbf{x}^T \to \lambda \mathbf{x}^T$ if it satisfies the homogeneity condition

$$F_i(\mathbf{y}(t)|\lambda \mathbf{x}^T) = \lambda^{\mu_i} F_i(\mathbf{y}(t)|\mathbf{x}^T), \tag{S21}$$

with $\mu_i \in \{1, 2, 3 \ldots\}$. In the following we identify the topological features of a chemotaxis pathway necessary for CheY-P to be invariant against variations in transcriptional activity.

We first investigate the Barkai-Leibler system shown in Fig 1a. To illustrate the point we assume that each receptor has only one methylation site. Methylated receptors are active with probability $p(L)$, with L the ambient ligand concentration. Non-methylated receptors

remain inactive with probability one. The set of differential equations for this system is given by

$$\partial_t T_M = k_R R \frac{T^T - T_M}{K_R + T^T - T_M} - k_B B \frac{T_A}{K_B + T_A} \tag{S22}$$

$$\approx k_R R - k_B B^T \frac{T_A}{K_B + T_A} \tag{S23}$$

$$\partial_t Ap = k_A T_A \left(A^T - Ap \right) - k_Y Ap \left(Y^T - Yp \right) \tag{S24}$$

$$\partial_t Yp = k_Y Ap \left(Y^T - Yp \right) - \gamma_Y Yp . \tag{S25}$$

The approximation resulting in Eq. (S23) is valid for $T^T - T_M \gg K_R$, i.e. for R working at saturation. Also, we assume that only active receptors can be demethylated. The dephosphorylation rate of CheY-P is given by γ_Y.

The steady state concentrations of the active components of this system are:

$$T_A = K_B \frac{k_R R}{k_B B^T - k_R R} \tag{S26}$$

$$Ap = \frac{k_A T_A A^T}{k_A T_A + k_Y \left(Y^T - Yp \right)} \approx \frac{k_A T_A}{k_Y} \cdot \frac{A^T}{Y^T} \tag{S27}$$

$$Yp = \frac{k_Y Ap \, Y^T}{k_Y Ap + \gamma_Y} \tag{S28}$$

Approximations made in Eq. (S27) are valid for $Y^T \gg Yp$ and $k_Y Y^T \gg k_A T_A$. Latter is equivalent to $A^T \gg Ap$, which means that the phosphotransfer from CheA-P to CheY is significantly faster than the autophosphorylation of CheA. Performing the transformation $\mathbf{x}^T \rightarrow \lambda \mathbf{x}^T$ on Eqs. (S26)-(S27) shows that the steady state concentration of the active form of the receptor T_A and of CheA-P remain unchanged, since we can eliminate λ in these equations. But in Eq.(S28), λ cannot be eliminated. Thus the steady state concentration of CheY-P increases with λ. This means that the Barkai-Leibler model shown in Fig.1a is not robust against variations in transcriptional activity.

For topologies Fig. 1b-1d there is a phosphatase $Z = $ [CheZ] that dephosphorylates activated CheY. For these topologies the dephosphorylation term of CheY-P is given by $k_Z Z^T Yp$. Therefore Eq.(S25) can be rewritten as:

$$\partial_t Yp = k_Y Ap \left(Y^T - Yp \right) - k_Z Z^T Yp \tag{S29}$$

This changes the steady state equation of CheY-P to:

$$Yp = \frac{k_Y Ap \, Y^T}{k_Y Ap + k_Z Z^T} \approx \frac{k_Y Ap}{k_Z} \cdot \frac{Y^T}{Z^T} \tag{S30}$$

The approximation made here is valid for $k_Z Z^T \gg k_Y Ap$, which is equivalent to $Y^T \gg Yp$. Now the transformation $\mathbf{x}^T \rightarrow \lambda \mathbf{x}^T$ leaves the steady state of CheY-P unchanged. So in order to be robust against variations in transcriptional activity, CheY-P has to have a phosphatase.

For topologies Fig. 1c, 1d the methylesterase CheB is only active if it is phosphorylated by Ap. Thus for these topologies we get an additional differential equation for $Bp = [\text{CheB-P}]$ given by

$$\partial_t Bp = k'_B \, Ap \, (B^T - Bp) - \gamma_B Bp, \qquad (S31)$$

with k'_B the rate of phosphotransfer from CheA-P to CheB and γ_B is the dephosphorylation rate of Bp. Technically the term $k'_B \, Ap \, (B^T - Bp)$ has to be considered also in Eq.(S24). But since $k_Y Y^T \gg k'_B \, B^T$, this term can be neglected. Then the steady state of this equation reads:

$$Bp = \frac{k'_B Ap \, B^T}{k'_B Ap + \gamma_B}. \qquad (S32)$$

Under the transformation $\mathbf{x}^T \to \lambda \mathbf{x}^T$ the steady state value for Bp increases by a factor λ. For the receptor activity to be invariant against transcriptional noise, the scaling of CheB-P with λ is a necessary condition, as can be seen from Eq. (S26) with CheB-P substituted for CheB.

Clearly, if CheB-P would have a phosphatase, its steady state would not scale with λ. This in turn would destroy the invariance of T_A. As a result, neither CheA-P nor CheY-P would be invariant under λ-fold increase in protein levels.

Also, an auto-methylation process of the receptors is no alternative to the methyltransferase CheR. Assuming auto-methylation as the main methylation process, we would have to substitute the term $k_R R$ in Eq. (S23) by $k_m(T^T - T_M)$, with k_m the automethylation rate. But then the homogeneity condition, Eq. (S21), would be violated.

Summarising we can say that in order for a topology to be robust against variations in transcriptional activity, the following conditions have to be fulfilled:

- a methyltransferase CheR has to exist and work at saturation,

- the dephosphorylation of CheY-P has to be taken over by a phosphatase CheZ, see Eq.(S30),

- CheB-P must not have a phosphatase

- CheA-P and CheY-P have to be significantly smaller than their total concentrations, i.e. $Ap \ll A^T$ and $Yp \ll Y^T$.

The consequences of the violation of these conditions are illustrated in Fig. S4. So far we have shown that the steady states of topologies Fig. 1b-1d are robust against variations in transcriptional activity. But what happens to the dynamics of a system under this transformation? Since the differential Eqs.(S23), (S24), (S29) and (S31) are linear in the concentrations $\{A^T, B^T, R, Y^T\}$ under the assumptions $A^T \gg Ap$, $Y^T \gg Yp$, the entire system $F_i(\mathbf{y}(t)|\mathbf{x}^T)$ is a linear function with respect to $\mathbf{x}^T$ and we can write:

$$\partial_t y_i = F_i(\mathbf{y}(t)|\lambda \mathbf{x}^T) = \lambda F_i(\mathbf{y}(t)|\mathbf{x}^T) = \lambda \partial_{t'} y_i \qquad (S33)$$

This means, a λ-fold increase in transcriptional activity results in a rescaling of time: $t' = \lambda t$. Now the dynamics of both systems are identical in different time-frames. Temperature changes, e.g., alter kinetic rate constants and result to first order also in a rescaling of time. Consequently the steady state values of the pathway are also invariant under moderate variations in the ambient temperature.

2.5. Alternative Feedback Loops

Within our modelling approach we also investigated an effect of several alternative hypothetical feedback loops (Fig. S5) on the chemotactic efficiency. The results of our simulations (not shown) support the analytical finding that: (i) a methyltransferase (CheR) has to exist, because auto-methylation of inactive receptors violates robustness against concerted variations in expression levels, although it satisfies the conditions for precise adaptation [11], (ii) a negative feedback loop, resulting from inactivation of CheR by phosphotransfer from CheA, shows only about half the efficiency for noise compensation of a feedback via CheB phosphorylation as a consequence of CheR working close to saturation and (iii) a negative feedback from CheY-P to the kinase activity through binding to the receptor complexes also violates robustness against co-variation in expression levels, which can only be repaired if CheY-P would bind exclusively to active receptors. Although the CheY-CheZ feedback loops in Fig. 1d and Fig. S5 lead effectively to a cooperative activity of CheZ with respect to CheY-P dephosphorylation, only in Fig. 1d the invariance of CheY-P against overexpression of CheY and CheZ is preserved.

2.6. Error Reduction Mechanisms

In this section we show how errors in the output signal arising from imperfection of components or independent variations of protein levels can partially be compensated by additional feedback loops and an optimal choice of kinetic parameters. In the following we look at the differential equations of the topologies of *E. coli* and the Barkai-Leibler system to show the difference in error reduction between topologies with and without additional feedback.

The differential equations for the topology in Fig. 1c for the receptor methylation T_M, the receptor protein $Ap = $ [CheA-P], the messenger protein $Yp = $ [CheY-P], and the methylesterase $Bp = $ [CheB-P] are given by

$$\partial_t T_M = k_R R - k_B Bp \, \frac{T_A}{K_B + T_A} \tag{S34}$$

$$\partial_t Ap = k_A \left(A^T - Ap \right) T_A - k_Y Ap \left(Y^T - Yp \right)$$
$$\quad - k_B' Ap \left(B^T - Bp \right) \tag{S35}$$

$$\partial_t Yp = k_Y Ap \left(Y^T - Yp \right) - k_Z Yp \, Z, \tag{S36}$$

$$\partial_t Bp = k_B' Ap \left(B^T - Bp \right) - \gamma_B Bp. \tag{S37}$$

In this topology, the demethylation of the receptor complex is performed only by the phosphorylated form of CheB. The phosphorylation of CheB results from phosphotransfer of CheA-P, where CheA is part of the receptor complex. Thus the activated form of CheB is a function of the activity of the receptor complex, and one has the functional form $Bp = Bp(Ap)$. This functional dependence gives an additional feedback to the system as shown in Fig. 1c.

For the Barkai-Leibler system, topology Fig.1a, the methylesterase of the receptor complex is active only in unphosphorylated form and does therefore not depend on the phosphorylation level of CheA, see Eqs. (S23)-(S25).

From the steady state of Eq.(S35) we can define the functional:

$$
\begin{aligned}
f(Ap, Bp, Yp, T_A) := \ & k_A \left(A^T - Ap\right) T_A - k_Y Ap \left(Y^T - Yp\right) \\
& - k'_B Ap \left(B^T - Bp\right),
\end{aligned}
\tag{S38}
$$

where the functions $T_A = T_A(Bp, R)$, $Yp = Yp(Ap, Y^T, Z)$ and $Bp = Bp(Ap)$ are derived from the steady states of Eqs.(S34),(S36) and (S37). We calculate the total differential of the functional f to get the sensitivity of the kinase activity of CheA-P with respect to changes in protein concentrations.

To get the dependence of Ap and R to linear order, one has to calculate the total differential of the functional in Eq.(S38)

$$
df = \frac{\partial f}{\partial Ap} dAp + \frac{\partial f}{\partial R} dR = 0,
\tag{S39}
$$

keeping all other protein concentrations constant. Solving this for dAp gives:

$$
\begin{aligned}
dAp \ &= \ -\left(\frac{\partial f}{\partial Ap}\right)^{-1} \frac{\partial f}{\partial R} dR \\[2mm]
&= \ -\frac{\dfrac{\partial f}{\partial T_A}\dfrac{\partial T_A}{\partial R}}{\left.\dfrac{\partial f}{\partial Ap}\right|_{T_A,Yp,Bp} + \dfrac{\partial f}{\partial Yp}\dfrac{\partial Yp}{\partial Ap} + \left(\left.\dfrac{\partial f}{\partial Bp}\right|_{T_A} + \dfrac{\partial f}{\partial T_A}\dfrac{\partial T_A}{\partial Bp}\right)\dfrac{\partial Bp}{\partial Ap}} dR
\end{aligned}
\tag{S40}
$$

The terms after the vertical lines indicate the concentrations kept constant for this derivative. Using the following definitions:

$$
\alpha := \left.\frac{\partial f}{\partial Ap}\right|_{T_A,Yp,Bp} + \frac{\partial f}{\partial Yp}\frac{\partial Yp}{\partial Ap}
\tag{S41}
$$

$$
\beta := \left.\frac{\partial f}{\partial Bp}\right|_{T_A} + \frac{\partial f}{\partial T_A}\frac{\partial T_A}{\partial Bp},
\tag{S42}
$$

we can simplify the representation of dAp to:

$$
dAp = -\frac{\dfrac{\partial f}{\partial T_A}\dfrac{\partial T_A}{\partial R}}{\alpha + \beta\dfrac{\partial Bp}{\partial Ap}} dR
\tag{S43}
$$

12

The term $\partial Bp/\partial Ap$ arises through the additional feedback and is zero for the Barkai-Leibler topology. In section 2.6.1 we show that α is always negative for $Yp < 0.75\,Y^T$. In section 2.6.2 we show that β is always negative for K_B being sufficiently large. Since $\partial Bp/\partial Ap > 0$, what can be seen from the steady state of Eq.(S37), the absolute value of the denominator of Eq.(S43) is larger for the topology with additional feedback than for the Barkai-Leibler model. This means, that fluctuations in the activity of $CheA - P$, that result from fluctuations of CheR, are minimised by the additional feedback loop. The error reduction by this additional feedback loop works better, the greater the absolute value of $\beta\partial Bp/\partial Ap$. As shown in section 2.6.4, the effectiveness of the error correction of the feedback increases with B^T/Bp.

Equivalently, these calculations can be done for the other protein concentrations , resulting in:

$$dAp = -\frac{\frac{\partial f}{\partial T_A}\frac{\partial T_A}{\partial R}}{\alpha + \beta\frac{\partial Bp}{\partial Ap}}dR \tag{S44}$$

$$dAp = -\frac{\frac{\partial f}{\partial Y^T}\big|_{Yp} + \frac{\partial f}{\partial Yp}\frac{\partial Yp}{\partial Y^T}}{\alpha + \beta\frac{\partial Bp}{\partial Ap}}dY^T \tag{S45}$$

$$dAp = -\frac{\frac{\partial f}{\partial Yp}\frac{\partial Yp}{\partial Z}}{\alpha + \beta\frac{\partial Bp}{\partial Ap}}dZ \tag{S46}$$

$$dAp = -\frac{\frac{\partial f}{\partial B^T}\big|_{T_A,Bp} + \beta\frac{\partial Bp}{\partial B^T}}{\alpha + \beta\frac{\partial Bp}{\partial Ap}}dB^T \tag{S47}$$

The numerator of Eqs. (S44-S46), are the same for the topology with additional feedback (Fig. 1c, 1d) and without (Fig. 1a, 1b). Thus, deviations from the optimal value of CheA-P arising through fluctuations of total proteins concentrations get attenuated by the additional feedback loop via CheB phophorylation.

In Eq. (S47), the value of the numerator of the simpler systems (Fig. 1a, 1b), $\partial f/\partial T_A \cdot \partial T_A/\partial B^T$, is different to the numerator of the systems with additional feedback, $\partial f/\partial B^T\big|_{T_A,Bp} + \beta \cdot \partial Bp/\partial B^T$. In section 2.6.3 we show that variations in the total concentration of CheB are reduced by the additional feedback loop whenever the denominator of Eqs. (S44-S47) increases by more than 1% compared to the denominator of the simpler systems, Fig. 1a, 1b.

2.6.1. Derivation of the Condition for $\alpha < 0$

In this section we derive the condition that has to be fulfilled for α to be negative.

$$
\begin{aligned}
\alpha &= \left. \frac{\partial f}{\partial Ap} \right|_{T_A, Yp, Bp} + \frac{\partial f}{\partial Yp} \frac{\partial Yp}{\partial Ap} \\
&= -k_A T_A - k_Y \left(Y^T - Yp \right) - k'_B \left(B^T - Bp \right) + k_Y Y^T \frac{k_Y Ap \, k_Z Z}{\left(k_Y Ap + k_Z Z \right)^2} < 0
\end{aligned}
$$

Since the phosphorylation of CheA is the rate limiting step in this reaction, $k_Y Y^T \gg k_A T_A$, we can neglect the term $k_A T_A$, [5]. Also, since $k_Y Y^T \gg k'_B B^T$, we can neglect the term $k'_B \left(B^T - Bp \right)$. Both simplification are conservative, i.e. they make the inequality even more strict. We get as a condition for $\alpha < 0$:

$$
\begin{aligned}
&-k_Y \left(Y^T - Yp \right) + k_Y Y^T \frac{k_Y Ap \, k_Z Z}{\left(k_Y Ap + k_Z Z \right)^2} < 0 \\
\implies\ & \frac{k_Y Ap \, k_Z Z}{\left(k_Y Ap + k_Z Z \right)^2} < \frac{Y^T - Yp}{Y^T} \\
\implies\ & \frac{\frac{k_Z Z}{k_Y Ap}}{\left(1 + \frac{k_Z Z}{k_Y Ap} \right)^2} < \frac{Y^T - Yp}{Y^T}
\end{aligned}
\tag{S48}
$$

There always exists a real number $\omega > -1$ such that $k_Z Z = (1 + \omega) k_Y Ap$. Thus inequality (S48) can be written as:

$$
\begin{aligned}
& \frac{1 + \omega}{(2 + \omega)^2} = \frac{1 + \omega}{4 + 4\omega + \omega^2} \leq \frac{1 + \omega}{4(1 + \omega)} = \frac{1}{4} < \frac{Y^T - Yp}{Y^T} \\
\implies\ & Y^T < 4Y^T - 4Yp \\
\implies\ & Yp < \frac{3}{4} Y^T
\end{aligned}
$$

Thus α is always negative for $Yp < 0.75\, Y^T$.

2.6.2. Derivation of the Condition for $\beta < 0$

From Eqs. (S44)-(S47) we can see that the error reduction mechanism of the chemotaxis topology works more efficiently if the denominator increases in magnitude. Since $\partial Bp / \partial Ap$ is positive and α is negative, β has to be smaller than zero for the additional feedback to have a positive noise reduction effect. Here we derive the conditions for β being smaller than zero:

$$
\beta = \frac{\partial f}{\partial T_A} \frac{\partial T_A}{\partial Bp} + \left. \frac{\partial f}{\partial Bp} \right|_T = k_A \left(A^T - Ap \right) \frac{\partial T_A}{\partial Bp} + k'_B Ap < 0
$$

From the steady state of Eq.(S34) one can see that $\frac{\partial T_A}{\partial Bp} < 0$, thus we have $\frac{\partial T_A}{\partial Bp} = -\left|\frac{\partial T_A}{\partial Bp}\right|$ and we get:

$$\left|\frac{\partial T_A}{\partial Bp}\right| = \frac{\frac{k_B}{k_R}\frac{K_B}{R}}{\left(\frac{k_B}{k_R}\frac{Bp}{R} - 1\right)^2} = \frac{\frac{k_B}{k_R}\frac{Bp}{R}}{\left(\frac{k_B}{k_R}\frac{Bp}{R} - 1\right)^2}\frac{K_B}{Bp} > \frac{k_B'\,Ap}{k_A\,(A^T - Ap)} \tag{S49}$$

Defining $\epsilon := k_B'Ap/(k_A(A^T - Ap))$ and $\gamma := k_B Bp/k_R R$ we get:

$$\frac{\gamma}{(\gamma - 1)^2}\frac{K_B}{Bp} > \epsilon$$

$$\iff K_B > \epsilon\,Bp\,\frac{(\gamma - 1)^2}{\gamma} \tag{S50}$$

From our simulations we have $\epsilon \approx 0.014$, as well as $(\gamma - 1)^2/\gamma \approx 7.5$ and $Bp \approx 0.09\,\mu M$. Thus for K_B larger than $0.01\,\mu M$ we can satisfy the condition $\beta < 0$.

2.6.3. Error reducing Effect on Variations of CheB

In order to show that the systems with additional feedback have an error reducing effect also on variations in the total concentration of CheB, we have to show that the absolute value of the term on the right hand side of Eq. (S47) is smaller for the systems with additional feedback, (Fig. 1c, 1d), compared to the simpler systems, (Fig. 1a, 1b). Thus, we have to show that:

$$\frac{\left.\frac{\partial f}{\partial B^T}\right|_{T_A, Bp} + \beta\frac{\partial Bp}{\partial B^T}}{\alpha + \beta\frac{\partial Bp}{\partial Ap}}$$

$$= \frac{\left.\frac{\partial f}{\partial B^T}\right|_{T_A, Bp} + \frac{\partial f}{\partial T_A}\frac{\partial T_A}{\partial Bp}\frac{\partial Bp}{\partial B^T} + \left.\frac{\partial f}{\partial Bp}\right|_{T_A}\frac{\partial Bp}{\partial B^T}}{\alpha + \beta\frac{\partial Bp}{\partial Ap}} < \frac{\frac{\partial f}{\partial T_A}\frac{\partial T_A}{\partial B^T}}{\alpha} \tag{S51}$$

Note that the term $\partial f/\partial T_A$ is equal for all topologies depicted in Fig. 1. One can easily see that both sides of this inequality are greater than zero, that is why we do not have to take the absolute value. This inequality can be rewritten as:

$$\frac{\frac{\partial f}{\partial T_A}\frac{\partial T_A}{\partial Bp}\frac{\partial Bp}{\partial B^T}}{\alpha} + \frac{\left(\left.\frac{\partial f}{\partial B^T}\right|_{T_A, Bp} + \left.\frac{\partial f}{\partial Bp}\right|_{T_A}\frac{\partial Bp}{\partial B^T}\right)\alpha - \left(\frac{\partial f}{\partial T_A}\frac{\partial T_A}{\partial Bp}\frac{\partial Bp}{\partial B^T}\right)\beta\frac{\partial Bp}{\partial Ap}}{\alpha\left(\alpha + \beta\frac{\partial Bp}{\partial Ap}\right)} < \frac{\frac{\partial f}{\partial T_A}\frac{\partial T_A}{\partial B^T}}{\alpha}$$

With $\partial T_A/\partial Bp \cdot \partial Bp/\partial B^T \approx \partial T_A/\partial B^T$ we get:

$$\frac{\left(\left.\frac{\partial f}{\partial B^T}\right|_{T_A, Bp} + \left.\frac{\partial f}{\partial Bp}\right|_{T_A}\frac{\partial Bp}{\partial B^T}\right)\alpha - \left(\frac{\partial f}{\partial T_A}\frac{\partial T_A}{\partial Bp}\frac{\partial Bp}{\partial B^T}\right)\beta\frac{\partial Bp}{\partial Ap}}{\alpha\left(\alpha + \beta\frac{\partial Bp}{\partial Ap}\right)} < 0$$

$$\implies \left(\left.\frac{\partial f}{\partial B^T}\right|_{T_A, Bp} + \left.\frac{\partial f}{\partial Bp}\right|_{T_A}\frac{\partial Bp}{\partial B^T}\right)\alpha - \left(\frac{\partial f}{\partial T_A}\frac{\partial T_A}{\partial Bp}\frac{\partial Bp}{\partial B^T}\right)\beta\frac{\partial Bp}{\partial Ap} < 0$$

15

From Eq.(S38), one can see that $\partial f/\partial Bp|_{T_A} = -\left.\partial f/\partial B^T\right|_{T_A,Bp}$, and we get:

$$\alpha \left(\left.\frac{\partial f}{\partial B^T}\right|_{T_A,Bp} + \left.\frac{\partial f}{\partial Bp}\right|_{T_A} \frac{\partial Bp}{\partial B^T} \right) = \alpha \left.\frac{\partial f}{\partial Bp}\right|_{T_A} \left(\frac{\partial Bp}{\partial B^T} - 1 \right)$$
$$< \left(\frac{\partial f}{\partial T_A} \frac{\partial T_A}{\partial Bp} \frac{\partial Bp}{\partial B^T} \right) \beta \frac{\partial Bp}{\partial Ap} \approx \left(\frac{\partial f}{\partial T_A} \frac{\partial T_A}{\partial B^T} \right) \beta \frac{\partial Bp}{\partial Ap} \tag{S52}$$

Dividing this inequality by $\alpha \cdot \left(\partial Bp/\partial B^T - 1\right)$, we get:

$$\left.\frac{\partial f}{\partial Bp}\right|_{T_A} < \frac{\partial f}{\partial T_A} \frac{\partial T_A}{\partial B^T} \frac{1}{\left(\frac{\partial Bp}{\partial B^T} - 1\right)} \frac{\beta \frac{\partial Bp}{\partial Ap}}{\alpha} \tag{S53}$$

With $\partial T_A/\partial B^T < 0$ and setting $\partial Bp/\partial B^T \approx 0$, what makes the inequality more strict, we get:

$$\left.\frac{\partial f}{\partial Bp}\right|_{T_A} < -\frac{\partial f}{\partial T_A} \frac{\partial T_A}{\partial B^T} \frac{\beta \frac{\partial Bp}{\partial Ap}}{\alpha} = \frac{\partial f}{\partial T_A} \left| \frac{\partial T_A}{\partial B^T} \right| \frac{\beta \frac{\partial Bp}{\partial Ap}}{\alpha} \tag{S54}$$

From simulations we can roughly estimate $\left| \frac{\partial T_A}{\partial B^T} \right| \approx 1$. Using Eq.(S38) we get:

$$\frac{k'_B Ap}{k_A(A^T - Ap)} = \epsilon \approx 0.01 < \frac{\beta \frac{\partial Bp}{\partial Ap}}{\alpha} \tag{S55}$$

From this inequality we can see, that the additional feedback loop has an error reducing effect on variations in CheB, as long as the increase of the absolute value of the denominator of Eqs. (S44-S47) due to the effect of the additional feedback loop is larger than $\sim 1\%$.

2.6.4. Condition for the Effectiveness of the Feedback

From Eqs.(S44)-(S47) we can see that the error reduction mechanism works better the larger the term $\beta\, \partial Bp/\partial Ap$ gets. For $\beta\, \partial Bp/\partial Ap$ we can write:

$$
\begin{aligned}
\beta\frac{\partial Bp}{\partial Ap} &= \left(\frac{\partial f}{\partial T_A}\frac{\partial T_A}{\partial Bp} + \frac{\partial f}{\partial Bp}\bigg|_T\right)\frac{\partial Bp}{\partial Ap} \\
&= \left(-k_A\left(A^T - Ap\right)\frac{\frac{k_B}{k_R}\frac{Bp}{R}}{\left(\frac{k_B}{k_R}\frac{Bp}{R} - 1\right)^2}\frac{K_B}{Bp} + k'_B\, Ap\right) \times \frac{k'_B\gamma_B B^T}{\left(k'_B\, Ap + \gamma_B\right)^2} \\
&= \left(-\mu\frac{\chi Bp}{(\chi Bp - 1)^2}\frac{1}{Bp} + \nu\right)\kappa B^T,
\end{aligned}
\tag{S56}
$$

where all Greek letters are independent of Bp:

$$
\begin{aligned}
\chi &= \frac{k_B}{k_R R} \\
\mu &= k_A\left(A^T - Ap\right)K_B \\
\nu &= k'_B\, Ap \\
\kappa &= \frac{k'_B\gamma_B}{\left(k'_B Ap + \gamma_B\right)^2}
\end{aligned}
$$

The error correction mechanism performed by the feedback is stronger the larger the absolute value of Eq.(S56) is. In section 2.6.2 we showed that $\beta < 0$. Thus the negative term in Eq.(S56) is the dominating term. The value of the term χBp is fixed by the condition in Eq.(S34). This is necessary for the system to be able to respond to changes in concentration of the ligand. Since all variables denoted by Greek letters are independent of Bp, and χBp is fixed, the term in Eq.(S56) increases with B^T/Bp. Thus the smaller Bp compared to B^T, the better the error correction mechanism of the additional feedback.

3.   TETHERING CELLS EXPERIMENTS

Tethering cell experiments provide a direct readout of the phenotypic differences in the adapted level of phosphorylated CheY-P. The variations in average time a cells spends rotating clockwise (CW bias) as a function of the concentration of CheY-P depends strongly on the steepness of the motor response curve (see Fig. 3b). The distribution of the CW bias among a small population of cells for different expression levels is shown in Fig. S6. Below the expression level of the wild type, only a small fraction of switching cells was observed. For example, at the expression level half of the wild-type, only five out of 25 cells were switching. Such large variance hampered a reliable determination of the mean and standard deviation. Also, since a CheY-P level could not be derived for non-switching cells, we were not able not make a direct quantitative comparison of the data with the model predictions at these expression levels.

[1] Swain, P. S. Efficient attenuation of stochasticity in gene expression trough post-transcriptional control. *J. Mol. Biol.* **344**, 965–976 (2004).

[2] Li, M. and Hazelbauer, G. L. Cellular stoichiometry of the components of the chemotaxis signaling complex. *J. Bacteriol.* **186**, 3687–3694 (2004).

[3] http://www.anat.cam.ac.uk/ comp-cell/.

[4] Hartwell, L. H., Hopfield, J. J., Leibler, S., and Murray, A. W. From molecular to modular cell biology. *Nature* **402**, 47–52 (1999).

[5] Sourjik, V. and Berg, H. C. Receptor sensitivity in bacterial chemotaxis. *Proc Natl Acad Sci USA* **99**, 123–127 (2002).

[6] Duke, T. A. J. and Bray, D. Heightened sensitivity of a lattice of membrane receptors. *Proc. Natl. Acad. Sci. USA* **96**, 10104–10108 (1999).

[7] Barkai, N. and Leibler, S. Robustness in simple biochemical networks. *Nature* **387**, 913–917 (1997).

[8] Sourjik, V. Receptor clustering and signal processing in E. coli chemotaxis. *Trends Microbiol.* **12**, 569–576 (2004).

[9] Wadhams, G. H. and Armitage, J. P. Making sense of it all: bacterial chemotaxis. *Nat. Rev. Mol. Cell Biol* **5**, 1024–1037 (2004).

[10] Webre, D. J., Wolanin, P. M., and Stock, J. B. Bacterial chemotaxis. *Curr. Biol.* **13**, 47–49 (2003).

[11] Mello, B. and Yuhai, T. Perfect and near-perfect adaption in a model of bacterial chemotaxis. *Biophys. J.* **84**, 2943–2956 (2003).

[12] Rao, C. V., Kirby, J. R., and Arkin, A. P. Design and diversity in bacterial chemotaxis: a comparative study in E. coli and Bacillus Subtilis. *PLoS Biology* **2**, 239–251 (2004).

[13] Blat, Y., Gillespie, G., Bren, A., Dahlquist, F. W., and Eisenbach, M. Regulation of phosphatase activity in bacterial chemotaxis. *J. Mol. Biol.* **284**, 1191–1199 (1998).

[14] Levit, M. N. and Stock, J. B. Receptor methylation controls the magnitude of stimulus-response coupling in bacterial chemotaxis. *J. Biol. Chem.* **277**, 36760–36765 (2002).

[15] Rao, C. V., Frenklach, M., and Arkin, A. P. An allosteric model for transmembrane signaling in bacterial chemotaxis. *J. Mol. Biol.* **343**, 291–303 (2004).

[16] Bray, D., Levin, M. D., and Morton-Firth, C. J. Receptor clustering as a cellular mechanism to control sensitivity. *Nature* **393**, 85–88 (1998).

[17] Sourjik, V. and Berg, H. C. Functional interactions between receptors in bacterial chemotaxis. *Nature* **428**, 437 (2004).

[18] Wadhams, G. H. and Armitage, J. P. Making sense of it all: Bacterial chemotaxis. *Nature Reviews* **5**, 1024–1037 (2004).

[19] Mello, B. A. and Tu, Y. Quantitative modeling of sensitivity in bacterial chemotaxis: The role of coupling among differnt chemoreceptor species. *Proc. Natl. Acad. Sci. U S A* **100**, 8223–8228 (2003).

[20] Shi, Y. and Duke, T. Cooperative model of bacterial sensing. *Phys. Rev. E* **58**, 6399–6406

(1998).

[21] Adaptive Simulated Annealing (ASA), http://www.ingber.com/.

[22] Cluzel, P., Surette, M., and Leibler, S. An ultrasensitve bacterial motor revealed by monitoring signaling proteins in single cells. *Science* **287**, 1652–1655 (2000).
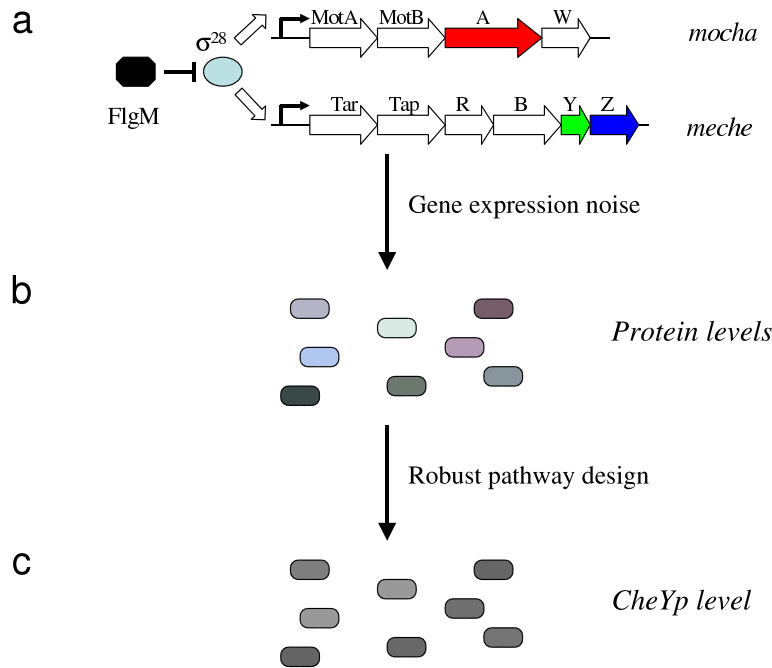
FIG. S1: Robustness of the chemotaxis pathway to gene expression noise. All cytoplasmic chemotaxis genes and two receptor genes are organized in two operons, mocha and meche. Promoters of both operons are positively controlled by a specific sigma factor, σ^{28} (FliA), and negatively controlled by an anti-sigma factor, FlgM, which binds to FliA and keeps it inactive. Another major receptor, Tsr, is under the same control (not shown). There is a strong intercellular variation in the expression of chemotaxis genes in a cell population, as indicated by varying intensity of three colours, corresponding to CheA, CheY, and CheZ. Such gene expression noise is characterised by a strong concerted variation in the levels of all proteins and only a weak uncorrelated variation, as indicated by the colour of the cells being close to grey. A robust pathway design is able to compensate for such variations, and the corresponding variation in the level of CheY-P - output of the pathway - is much smaller than the variation in protein levels.
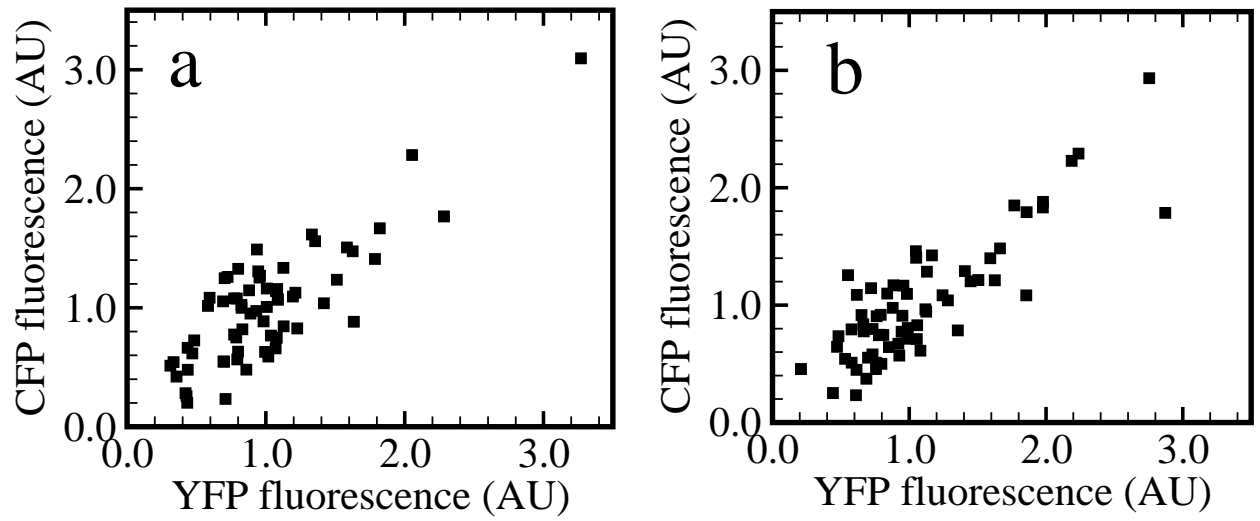
FIG. S2: Single-cell levels of CheY-YFP and CheZ-CFP co-expressed from a single IPTG-inducible promoter (pVS88). **a**, Mean expression level in absence of IPTG. **b**, gene expression noise generated *in silico* by Eq. (S17) with $\nu = 0.2$ and $\alpha = 0.2$.
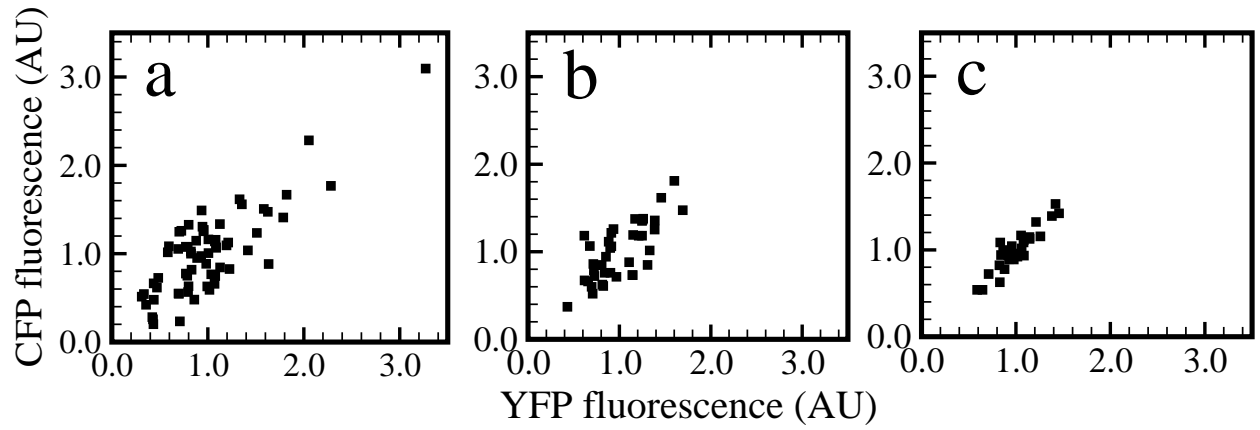
FIG. S3: Gene expression noise of CheY-YFP and CheZ-CFP co-expressed from pVS88 as in Fig. 1S at 0μM (**a**), 5μM (**b**), and 10μM (**c**) IPTG. Fluorescence values for each induction level are normalized to the mean expression levels, 1, 2.5, and 14, respectively. The corresponding values for intrinsic and extrinsic noise are given in Table 1.
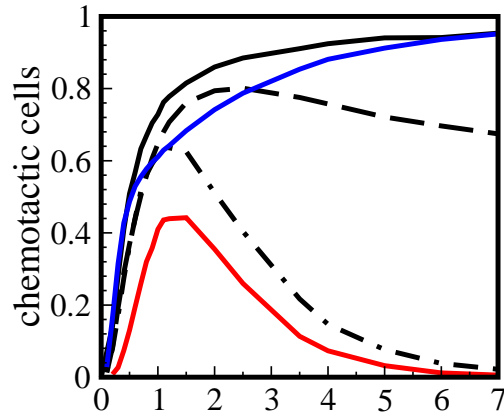
FIG. S4: Fraction of chemotactic cells from computer simulations in a population of 10^4 individuals under wild-type gene expression noise. Black line: topology Fig. 1c; dashed line: topology Fig. 1c, but with CheR binding with Michaelis-Menten constant $K_R = 3\mu M$ to the receptor complex; dashed-dotted line: topology Fig. 1c, but with a phosphatase substituting auto-dephosphorylation of CheB-P; red line: BL topology Fig. 1a; blue line: topology Fig. 1b.
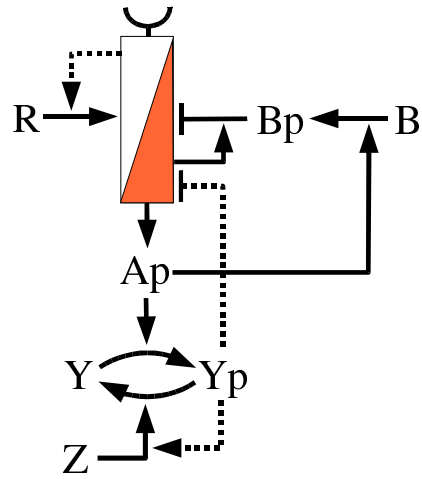
FIG. S5: Same as the *E. coli* topology Fig. 1c with additional hypothetical feedback loops drawn as dashed lines: (i) CheR works on inactive receptors with a given Michaelis-Menten constant, (ii) allosteric recruitment of CheZ by CheY-P without building an active form Z^*, and (iii) direct regulation of the receptor activity by binding of CheY-P to the receptor complexes.
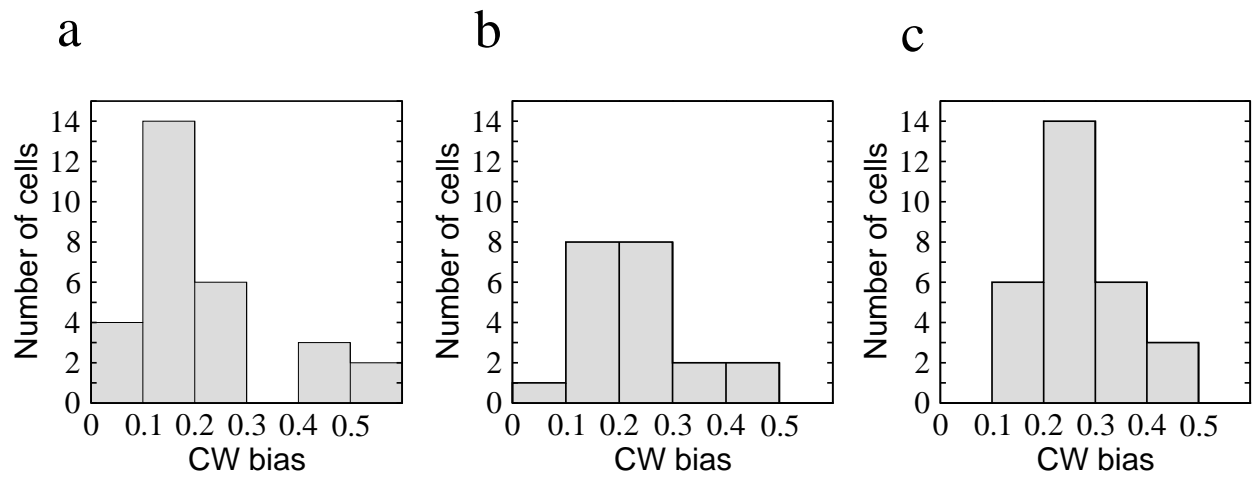
FIG. S6: Histogram of the CW bias distribution for populations having different expression levels of chemotaxis proteins. **a** wild type cells, **b** IPTG induceable cells with 3.2 fold wild type expression, **c** FlgM minus strain with 6.6 fold wild type expression

26